Applied Catalysis B: Environmental 140–141 (2013) 258–264

Contents lists available at SciVerse ScienceDirect

Applied Catalysis B: Environmental

journal homepage: www.elsevier.com/locate/apcatb

Study of Ru—Ni/TiO_2 catalysts for selective CO methanation

Shohei Tada [a], Ryuji Kikuchi [a,*], Atsushi Takagaki [a], Takashi Sugawara [a], S.Ted Oyama [a], Kohei Urasaki [b], Shigeo Satokawa [b]

[a] Department of Chemical System Engineering, School of Engineering, The University of Tokyo, 7-3-1 Hongo, Bunkyo-ku, Tokyo 113-8656, Japan
[b] Department of Materials and Life Science, Faculty of Science and Technology, Seikei University, 3-3-1 Kichijoji-Kitamachi, Musashino-shi, Tokyo 180-8633, Japan

ARTICLE INFO

Article history:
Received 7 January 2013
Received in revised form 20 February 2013
Accepted 9 April 2013
Available online 17 April 2013

Keywords:
Ruthenium
Nickel
Titania
Selective CO methanation
CO removal process

ABSTRACT

The removal of CO from reformate streams by selective CO methanation was investigated over TiO_2 supported Ru—Ni bimetallic and monometallic catalysts. The combination of Ru and Ni enhanced CO methanation at low temperatures. The introduction of Ni into Ru/TiO_2 decreased the CO_2 conversion rate at 260 °C from 10 to 7.3 μmol min^{-1} $g_{cat}{}^{-1}$. The use of Ru and Ni, thus, expands the temperature range of selective CO methanation. Transmission electron microscopy and temperature programmed reduction by H_2 confirmed that Ru species were in close proximity to Ni species on Ru—Ni/TiO_2, indicating a decrease in direct contact between Ru and TiO_2. Fourier transform infrared spectroscopy techniques revealed that the decomposition of the formate species, formed during CO_2 methanation, is slow over Ru—Ni/TiO_2, in contrast to Ru/TiO_2.

1. Introduction

Polymer electrolyte fuel cells (PEFCs) operate at low temperature (ca. 80 °C) and have received attention because of their high power densities and ease in start-up and shut-down. Carbon monoxide (CO) contained in reforming gases easily poisons the anode of PEFCs operating at such low temperatures. It is, therefore, imperative to reduce the CO concentration to below at least 100 ppm [1,2]. A large amount of CO in the reformates can be reduced from ca. 10% to 0.2–2% by water gas shift reaction (WGS reaction, $CO + H_2O \rightarrow CO_2 + H_2$) [3–5]. Preferential oxidation of CO in the presence of excess H_2 (PROX, $CO + 1/2O_2 \rightarrow CO_2$) following the WGS reaction can be utilized to abate CO to CO-tolerate level of the PEFC anode [6–9]. However, during PROX hydrogen is also easily oxidized in the presence of oxygen, leading to a decrease in the PEFC energy conversion efficiency.

As an alternative to PROX, CO methanation ($CO + 3H_2 \rightarrow CH_4 + H_2O$ (g), $\Delta H^{\circ}_{298} = -206$ kJ mol^{-1}) is regarded as a promising CO removal technique [10–25]. The advantages of CO methanation are that the reactants for this reaction (CO and H_2) are present in the reformate, and the produced CH_4 does not interfere with the PEFC performance. Furthermore the CH_4 can be used as a heating fuel for the reforming unit. The competing reactions of H_2 and CO_2 which include CO_2 methanation ($CO_2 + 4H_2 \rightarrow CH_4 + 2H_2O$ (g), $\Delta H^{\circ}_{298} = -165$ kJ mol^{-1}) and the reverse water-gas shift reaction (RWGS reaction, $CO_2 + H_2 \rightarrow CO + H_2O$ (g), $\Delta H^{\circ}_{298} = 41$ kJ mol^{-1}) are undesirable in CO removal because they consume H_2 and cause a runaway of the reactor. To obtain a wide operating temperature window for selective CO methanation, suitable catalysts must be developed that carry out CO methanation at low temperatures and do not favor CO_2 methanation and the RWGS reaction at high temperatures.

A great deal of effort has been made in studies of selective CO methanation in the presence of CO_2 and H_2O over Ru/Al_2O_3 [11–15], Ru/TiO_2 [11–14,17], Ni/TiO_2 [14,18], Ru/zeolite [19–22], and Ru/carbon nanofiber [25]. Recently Chen et al. have reported that 1 wt% Ru catalysts supported on mesoporous Ni—Al oxides (33 and 40 mol% Ni) exhibited high activity and selectivity in CO methanation [23]. While Ru addition to the Ni—Al oxides enhanced the reducibility of Ni species and the selectivity in CO methanation, the Ru species on the Ni—Al oxides were not characterized, and thus the actual effect of Ru and Ni species on selective CO methanation is not fully understood.

In our previous work, the effects of support materials and active species on selective CO methanation were investigated, and as for supported Ru catalysts, the interfaces of Ru and the supports were identified as the active sites for CO_2 methanation under conditions of coexisting CO and CO_2 [24]. Decreasing the interfacial contact is, therefore, important to suppress CO_2 methanation. It is reported

* Corresponding author. Tel.: +81 3 5841 1167; fax: +81 3 5841 1167.
E-mail address: rkikuchi@chemsys.t.u-tokyo.ac.jp (R. Kikuchi).

0926-3373/$ – see front matter © 2013 Elsevier B.V. All rights reserved.
http://dx.doi.org/10.1016/j.apcatb.2013.04.024

that CO methanation over supported metal catalysts proceeds via the dissociation of CO on the metal and the successive hydrogenation of the resultant surface carbonaceous species [26–29]. Increase of H_2 adsorbed dissociatively on metal species is likely to enhance the CO methanation activity. In this study, selective CO methanation over TiO_2-supported Ru—Ni bimetallic and monometallic catalysts was carried out, and the effect of the Ni additive on the activity and selectivity for CO methanation was investigated. The Ni metallic additive is expected to have the following two functions: (1) supply hydrogen to the Ru species (resulting in improvement of CO methanation) and (2) reduce the direct contact between Ru and TiO_2 (resulting in suppression of CO_2 methanation).

2. Experimental

2.1. Catalysis preparation

Ru/TiO_2 and Ni/TiO_2 catalysts were prepared by an impregnation method, and $Ru—Ni/TiO_2$ by a co-impregnation method. The TiO_2 support (JRC-TIO4), comparable to Degussa P25, was provided by the Catalysis Society of Japan. It was impregnated with an aqueous solution of $Ni(NO_3)_2{\cdot}6H_2O$ (Wako, 99.9%) and 3.920 wt% $Ru(NO_3)_3$ solution (Tanaka Co.). All samples were dried at 100 °C and then calcined at 500 °C for 3 h in air. The loadings of Ru and Ni were 0.5 and 5 wt%, respectively.

2.2. Activity test

The catalytic performance for selective CO methanation was evaluated in a 4-mm I.D. fixed-bed quartz tubular reactor at atmospheric pressure. The reaction temperature was measured at the inlet of the catalyst bed by a K-type thermocouple. A quantity of 300 mg of catalyst powder was placed in the reactor, and then reduced at 450 °C for 30 min in 5% H_2/Ar flow prior to each run. The feed gas, which simulates the methane reformate equilibrated at 190 °C, consists of 0.154% CO, 15.5% CO_2, 62.3% H_2 and 22.0% H_2O (dry base: 0.198% CO, 19.9% CO_2, 79.9% H_2). The gaseous mixture was fed at a space velocity of 11,000 h^{-1} (ca. 60–65 ml min^{-1}). The gas composition at the reactor outlet was analyzed with a micro gas chromatograph (Varian, CP-4900) equipped with MS-5A, COX and PPQ columns and a thermal conductivity detector (TCD). The outlet gas concentrations of CO, CO_2, CH_4, and H_2 were described on the basis of the dry gas composition. The conversion and conversion rate of x species (x = CO or CO_2) is defined as follows:

$$\text{Conversion of } x \text{ species} = 1 - \frac{F_{x,out}}{F_{x,in}} \quad (1)$$

$$\text{Conversion rate of } x \text{ species} = \frac{F_{x,in} \times \text{Conversion of } x \text{ species}}{W} \quad (2)$$

where $F_{x,in}$ and $F_{x,out}$ are the inlet and outlet molar flow rates of x species, respectively, and W is the catalyst weight.

2.3. Characterization

The specific surface area of each as-prepared catalyst was evaluated by the BET method using nitrogen adsorption (Micromeritics, ASAP2000). Temperature programmed reduction by H_2 (H_2-TPR) was carried out in a flow system (Quantachrome, CHEMBET-3000). About 25 mg of as-prepared samples were flushed initially with He flow at 300 °C and cooled to room temperature. A gaseous mixture of 5% H_2/Ar was fed to the reactor at 30 ml min^{-1}. The temperature was raised at a heating rate of 10 °C min^{-1}. The loading amount of Ru and Ni on each catalyst was determined by H_2 consumption in TPR measurements and inductively coupled plasma atomic emission spectrometry (ICP-AES, *SII* NanoTechnology, SPS4000).

The crystalline phase of catalysts was determined by X-ray diffraction (XRD) (Rigaku, RINT 2400 instrument) at voltage of 40 kV and current of 100 mA. Before XRD measurements, samples were reduced at the desired temperature in 5% H_2/Ar for 30 min, and mounted on the sample holder in air. The mean crystallite size of metallic Ni was estimated from the XRD patterns using the Scherrer equation,

$$D = \frac{K\lambda}{\beta \cos\theta} \quad (3)$$

where K is the shape factor (0.89), λ is X-ray wavelength (0.154 nm), β is the line broadening at half the maximum intensity in radians, and θ is Bragg's angle [30].

Transmission electron microscopy (TEM, JEOL-2010F) was used to determine the morphology of the Ru and Ni particles on the catalysts, and field emission scanning electron microscopy (FE-SEM; Hitachi, FE-SEM S-900) that of TiO_2. Additionally, X-ray energy dispersive spectrometry (EDS) was used to determine the elemental composition.

2.4. FTIR measurement

Fourier transform infrared (FTIR) spectroscopy measurements were performed to identify the intermediates of CO_2 methanation. The FTIR cell equipped with high purity CaF_2 windows and capability for heating and cooling was placed in a JASCO FTIR 6100 instrument with a mercury cadmium telluride detector (JASCO, MCT6000M). The powdered samples, reduced at 450 °C for 30 min under 5% H_2/Ar flow, were pressed into a thin self-supporting disk of about 20 mg cm^{-2} and set in the cell. The samples were oxidized during the disk preparation, but it was confirmed by H_2-TPR that the oxide layers could be reduced below 300 °C. All samples were pretreated in the cell by reduction at 350 °C in 5% H_2/Ar for 30 min, and cooling to 200 °C under N_2 atmosphere. Then background spectra were collected at 200 °C. The samples were exposed to the reaction gas ($CO_2/H_2/N_2$ = 2/15/83) for 60 min at 200 °C, and then their spectra were recorded after the mixed gas had been removed by flushing 10 min with N_2. The behavior of the CO_2 methanation intermediates was first investigated in inert gas. After reaction, the samples were exposed to N_2 gas at 200 °C, and then their spectra were measured. Typically, 200 scans were collected for one spectrum, and the results are presented as absorbance spectra. The behavior was also examined in hydrogen gas. The samples were exposed to the reaction gas (CO_2/H_2/Ar = 2/19/79) for 60 min at 200 °C, and 5% H_2/Ar gas at 200 °C, and then their spectra were measured. Typically, 50 scans were collected for one spectrum.

3. Results and discussion

In Fig. 1(a) CO concentration in methanation reaction over TiO_2-supported catalysts is plotted against reaction temperature. The order of activity for CO methanation was $Ru—Ni/TiO_2 > Ru/TiO_2 > Ni/TiO_2$. The CO concentration decreased rapidly with temperature over the three catalysts. Over $Ru—Ni/TiO_2$ the CO concentration fell to 460 ppm at 190 °C, over Ru/TiO_2 it decreased to 580 ppm at 200 °C, while for Ni/TiO_2 it dropped to 340 ppm at 215 °C. Over each catalyst, no CO production was detected at high temperatures, which means that the reaction rate of CO methanation is faster than that of the RWGS reaction.

Fig. 1(b) illustrates the CO_2 conversion curves over the TiO_2-supported catalysts as a function of reaction temperature. Over Ru/TiO_2 there was a steep increase in CO_2 conversion at temperatures above 225 °C. Over Ni/TiO_2 the conversion remained unchanged up to 260 °C, and then started to increase. For $Ru—Ni/TiO_2$ the CO_2 conversion curve was shifted to slightly higher temperature compared to that of Ru/TiO_2. The order of a CO_2

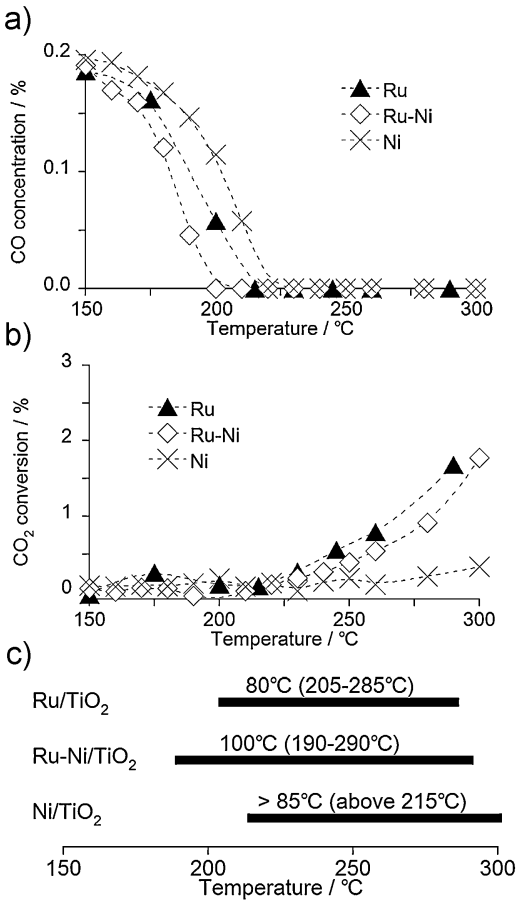

Fig. 1. (a) CO concentration and (b) CO_2 conversion over 0.5 wt%Ru/TiO_2, 0.5 wt%Ru—5 wt%Ni/TiO_2, and 5 wt%Ni/TiO_2 reduced at 450 °C. (c) Temperature window for selective CO methanation of TiO_2 supported Ru—Ni bimetallic and monometallic catalysts. Definition of window: CO concentration <500 ppm and CH_4 concentration <5000 ppm.

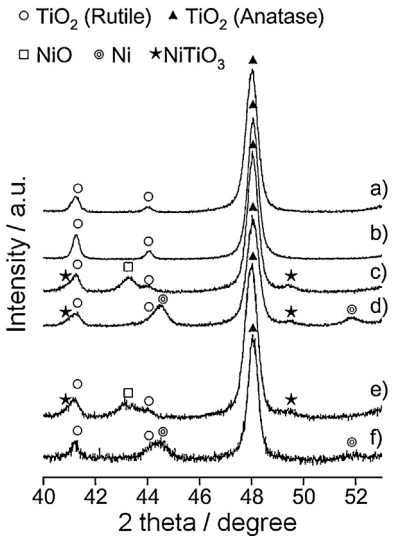

Fig. 2. XRD spectra of (a) TiO_2 (JRC-TIO4), (b) Ru/TiO_2 before reduction, (c) Ni/TiO_2 before reduction, (d) Ni/TiO_2 reduced at 450 °C, (e) Ru—Ni/TiO_2 before reduction, and (f) Ru—Ni/TiO_2 reduced at 450 °C. JCPDS-card number: NiO (47-1049), Ni (04-0850), rutile-type TiO_2 (21-1276), anatase-type TiO_2 (65-5714), and $NiTiO_3$ (76-0334).

conversion rate at 260 °C was Ru/TiO_2 > Ru—Ni/TiO_2 > Ni/TiO_2, as summarized in Table 1, which means that the Ni component of Ru—Ni/TiO_2 suppressed CO_2 methanation at high temperatures. Over all catalysts, the CO_2 conversion rose rapidly after CO was completely removed, as expected from the inhibitory effect of CO on CO_2 methanation even in a quite small amount [24,31].

Fig. 1(c) summarizes the temperature window for selective CO methanation in which CO and CH_4 concentrations are less than 500 and 5000 ppm, respectively. Under these conditions, H_2 conversion is estimated to be less than 2.2%. Catalysts for selective CO methanation are required to have a wide temperature window at a low temperature range for application in CO removal units in commercial PEFC systems. It is noteworthy that the temperature window of Ru—Ni/TiO_2 was broadened and shifted to lower temperature compared to Ru/TiO_2, which was the most active and selective for CO methanation in our previous report [24]. The temperature window of Ni/TiO_2 is located in a higher temperature range than that of Ru/TiO_2, with a slight expansion of the window.

To investigate the crystalline phases and the reduction extent of the Ru and Ni components in the catalysts, powder XRD measurements of TiO_2, Ru/TiO_2, Ni/TiO_2 and Ru—Ni/TiO_2 were performed, as shown in Fig. 2. Both rutile and anatase phases were identified in the TiO_2 supports used in these 6 samples, and the XRD patterns for the samples were not affected by reduction treatment. No Ru peaks were detected in the XRD patterns of Ru/TiO_2 and Ru—Ni/TiO_2, indicating that Ru species are in an amorphous state or that the Ru particle size is smaller than the XRD limit (4 nm). Peaks assignable to NiO at 43.2°, metallic Ni at 44.5 and 51.9°, and $NiTiO_3$ at 40.5 and 49.5° were observed. In Fig. 2(c) and (e), the patterns for unreduced Ni catalysts showed diffraction peaks of NiO. After reduction at 450 °C, the peaks attributed to NiO disappeared, and those of metallic Ni were detected (Fig. 2(d) and (f)). It is, therefore, expected that NiO was easily reduced at 450 °C prior to the reaction tests. In Table 1, the crystallite sizes of metallic Ni in Ni/TiO_2 and Ru—Ni/TiO_2 reduced at 450 °C were 19 and 22 nm, respectively, estimated from the (1 1 1) peak at 44.5° in the XRD pattern. The crystal phase and

Table 1
Loading weights, particle sizes, and crystallite sizes of Ru and Ni on TiO_2, and specific surface areas, and CO_2 conversion rates of TiO_2 supported Ru and/or Ni catalysts.

Catalysts	Loading weight [wt%]				Specific surface area[c] [$m^2\ g^{-1}$]	Particle size[d] [nm]		Crystallite size of Ni (1 1 1)[e] [nm]	CO_2 conv. rate at 260 °C[$\mu mol\ min^{-1}\ g_{cat}^{-1}$]
	ICP-AES		H_2-TPR						
	Ru	Ni	Ru[a]	Ni[b]		Ru	Ni		
Ru/TiO_2	0.44	–	0.49	–	45	3.4	–	–	10
Ru—Ni/TiO_2	0.39	4.1	0.37	3.9	43	1–3	10–20	22	7.3
Ni/TiO_2	–	4.6	–	4.8	47	–	22	19	1.4

[a] RuO_2 reduction was assumed.
[b] NiO or $NiTiO_3$ reduction was assumed.
[c] After reduction at 450 °C.
[d] Estimated from TEM images.
[e] Estimated by XRD patterns.

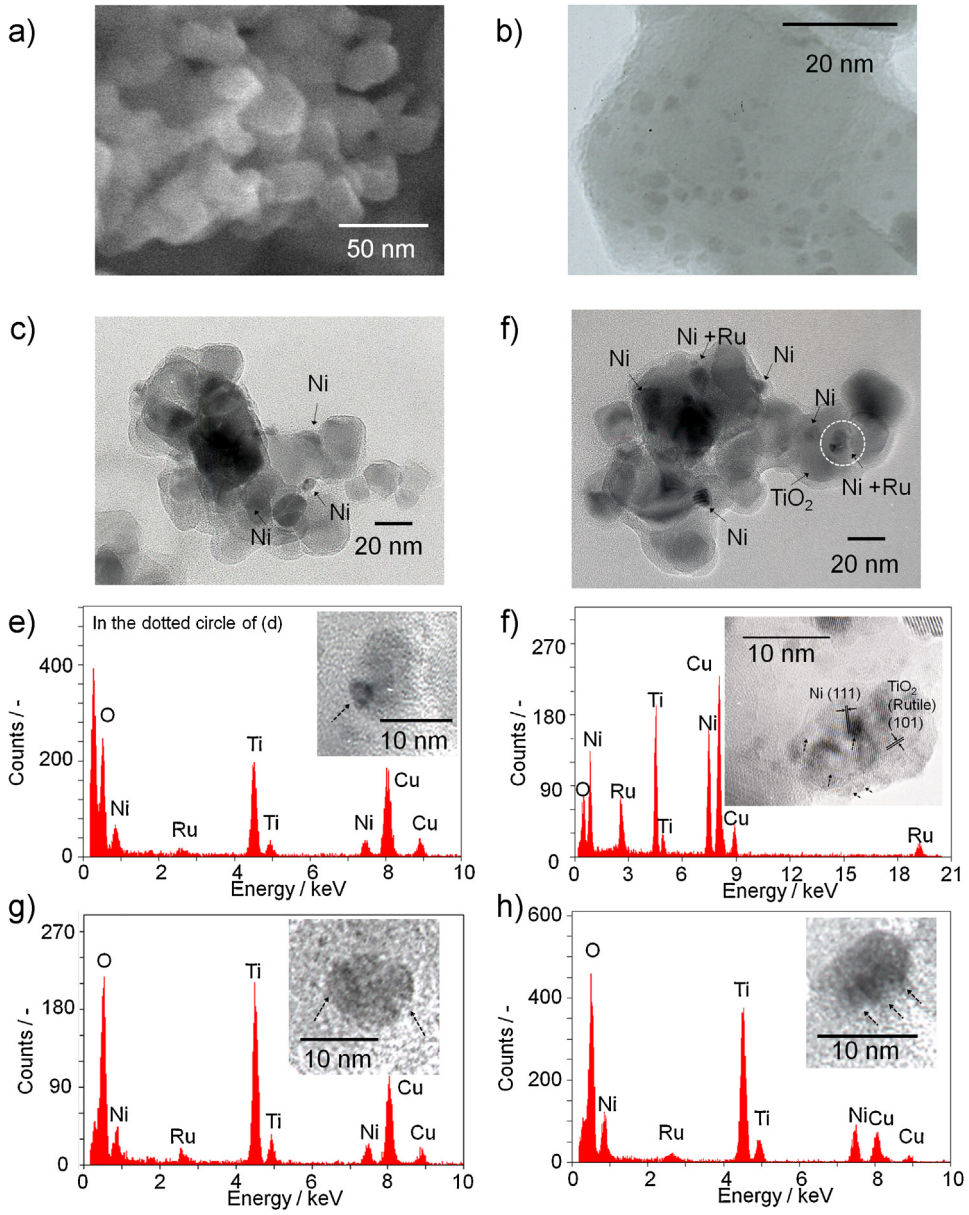

Fig. 3. (a) A SEM image of TiO_2. TEM images of (b) Ru/TiO_2, (c) Ni/TiO_2, and (d)–(h) $Ru—Ni/TiO_2$.

crystallite size of Ni species on Ni/TiO_2 was almost the same as that on $Ru—Ni/TiO_2$.

The BET specific surface areas of Ru/TiO_2, $Ru—Ni/TiO_2$, and Ni/TiO_2 determined by N_2 adsorption are listed in Table 1. The surface areas were similar to that of the original support ($47\ m^2\ g^{-1}$), indicating that the Ni and Ru compounds did not cause sintering or pore blockage.

As illustrated in Fig. 3, field emission-scanning electron microscopy (FE-SEM) was used to study the TiO_2 support, while transmission electron microscopy (TEM) and energy dispersive spectroscopy (EDS) were used to examine the Ru/TiO_2, Ni/TiO_2 and $Ru—Ni/TiO_2$ samples. Fig. 3(a) indicates that the average TiO_2 particle size was 30 nm. Fig. 3(b) shows a number of dark spots (3.4 nm on average) which are identified as Ru metal particles by EDS analysis. Fig. 3(c) displays large fractions of Ni particles (22 nm on average) supported on TiO_2. Fig. 3(d)–(h) shows a composite structure composed of dark particles of size about 10 nm and much darker clusters of size about 1–3 nm (indicated by dotted arrows), which means that this structural motif was common. Fig. 3(f) displays overlapping lattice fringes whose spacings are 0.20 nm and 0.25 nm and which are attributable to Ni (1 1 1) and rutile-type TiO_2 (1 0 1) crystalline plane, respectively. Fig. 3(d) shows that Ni, and Ru—Ni composite particles are supported on TiO_2. The EDS analyses

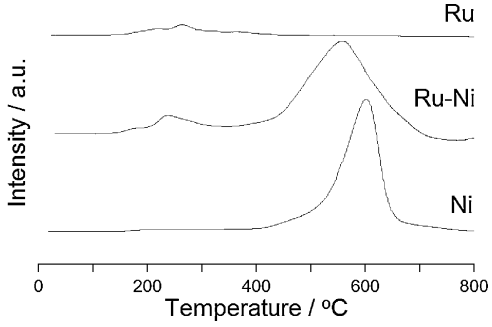

Fig. 4. H_2-TPR profiles of Ru/TiO_2, $Ru—Ni/TiO_2$, and Ni/TiO_2 ($\beta = 10\ ^\circ C\ min^{-1}$).

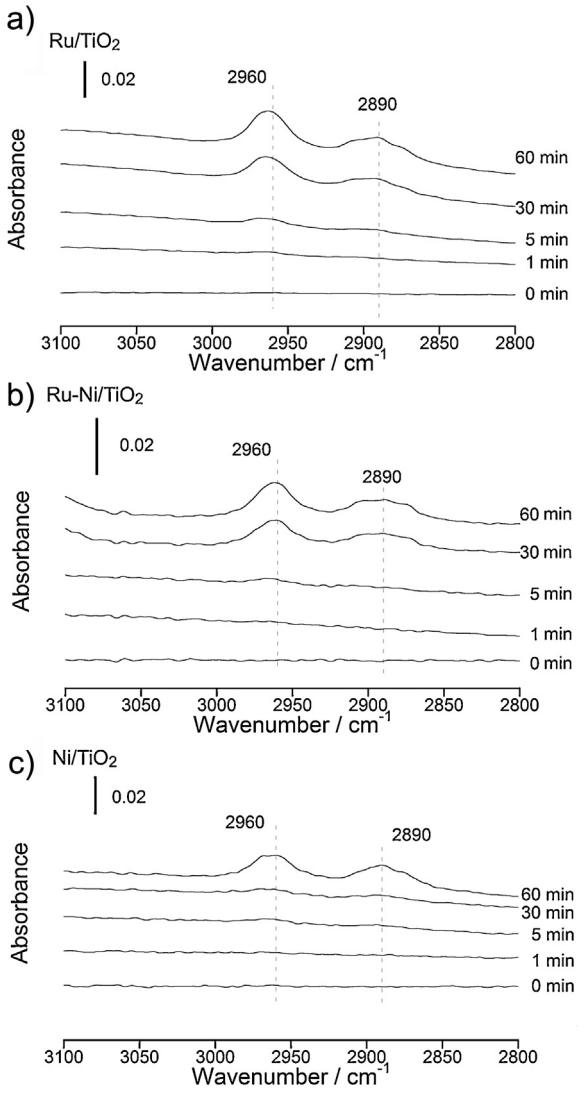

Fig. 5. FTIR spectra (200 scans each, 4 cm^{-1} resolution) in the high wavenumber range of (a) Ru/TiO_2, (b) Ru—Ni/TiO_2, and (c) Ni/TiO_2 during CO_2 methanation with the model gas mixture at 200 °C. The spectra were obtained in the following manner: reaction for desired time, and flushing 10 min with N_2.

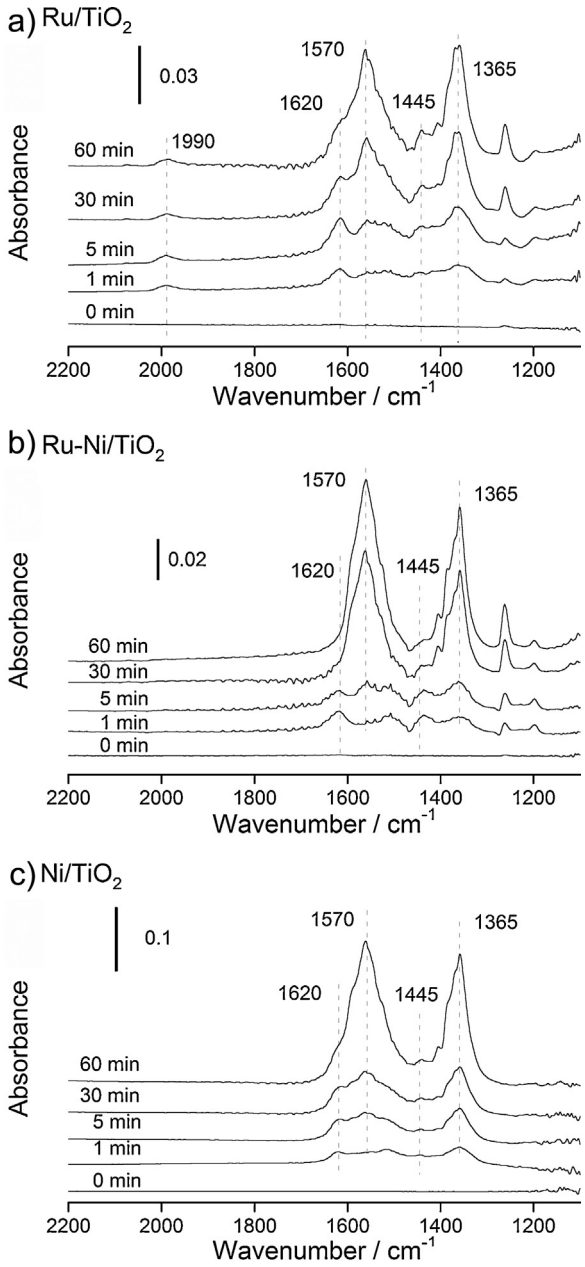

Fig. 6. FTIR spectra (200 scans each, 4 cm^{-1} resolution) in the low wavenumber range of (a) Ru/TiO_2, (b) Ru—Ni/TiO_2, and (c) Ni/TiO_2 during CO_2 methanation with the model gas mixture at 200 °C. The spectra were obtained in the following manner: reaction for desired time, and flushing 10 min with N_2.

of Fig. 3(e)–(h) revealed that the center particles included Ru and Ni species. Thus it is concluded that Ru particles of a few nm are located in close contact with Ni particles.

Fig. 4 shows the H_2-TPR profiles of the TiO_2-supported catalysts. In the case of the Ru-containing catalysts, a reduction peak was detected at around 220 °C, which has been ascribed in part to reduction of Ru oxides [32–35]. For the Ni catalyst, a single significant peak at around 550 °C can be assigned to reduction of NiO to metallic Ni [36–38]. The loading amount of Ru and Ni in each sample was estimated using H_2-TPR results, as summarized in Table 1. H_2 consumption was calculated by assuming reduction of Ru^{4+} (RuO_2) to Ru^0 and Ni^{2+} (NiO or $NiTiO_3$) to Ni^0. The loading amounts of Ru and Ni determined by H_2-TPR are close to those measured by ICP-AES, which indicates complete reduction of the metallic components. In addition, it was found that the Ni loading was almost the same over Ni/TiO_2 and Ru—Ni/TiO_2.

The reduction peak of NiO in the H_2-TPR profiles was shifted to lower temperature by adding Ru to Ni/TiO_2, indicating that the Ni reducibility was enhanced due to the presence of Ru. There are three possible explanations for the improved reducibility of Ni on Ru—Ni/TiO_2. The first possibility is a particle-size effect of NiO, with larger NiO particles reducible at lower temperatures due to weaker interactions with the support. As described above, however, the Ni species on Ru—Ni/TiO_2 had almost the same structure, morphology and loading amount, as those on Ni/TiO_2. The second possibility is the formation of bimetallic Ru—Ni cluster or alloy [39]. Crisafulli et al. discussed the effect of addition of Ru to Ni/SiO_2 catalysts on the CO_2 reforming of methane [40,41]. The Ru addition to supported Ni catalysts drastically enhanced the catalytic performance of the reaction. Moreover they characterized the CO adsorbed on the surface of silica supported monometallic and bimetallic Ru—Ni catalysts using FTIR. Over the bimetallic Ru—Ni catalyst the peaks attributed to CO adsorbed on Ni species appeared, but those on Ru species were not detected. In the H_2-TPR profile of the bimetallic catalyst, a Ru-related peak disappeared and a Ni-related one was shifted to lower temperatures in comparison

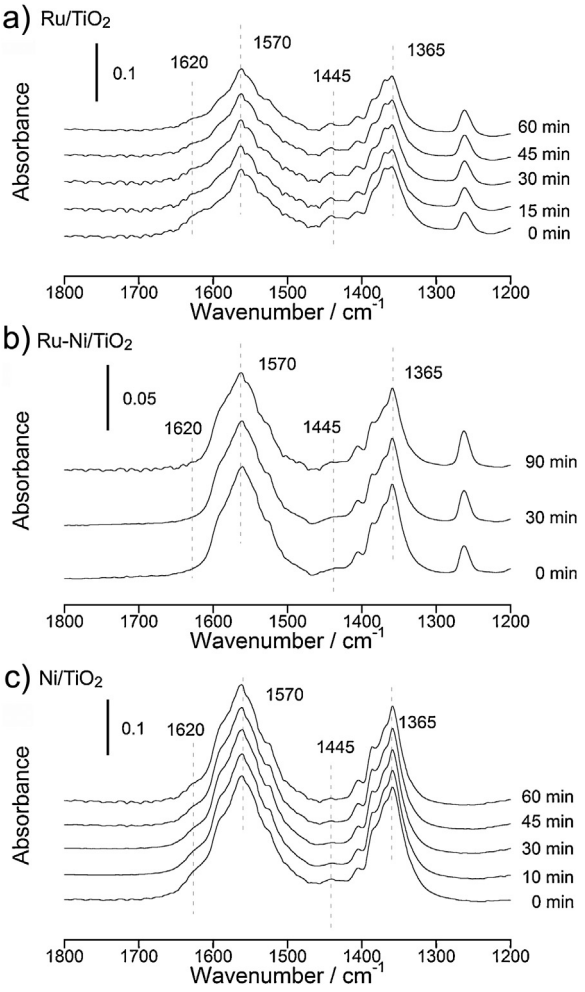

Fig. 7. FTIR spectra of (a) Ru/TiO_2, (b) Ru—Ni/TiO_2, and (c) Ni/TiO_2 after CO_2 methanation for 60 min at 200 °C. These spectra were recorded after a switch from the model gas mixture for CO_2 methanation to N_2.

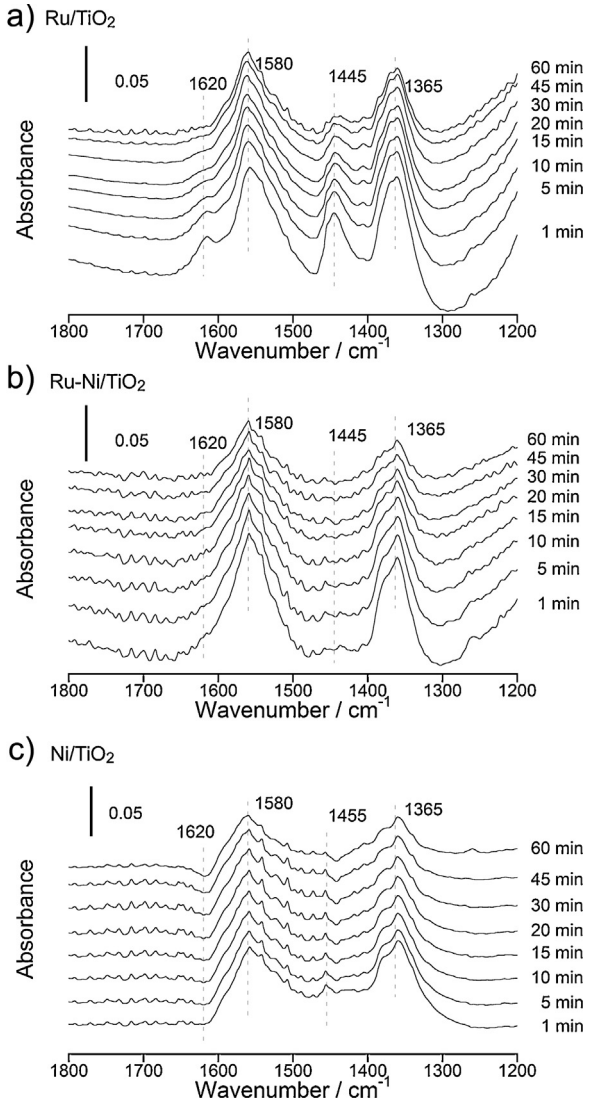

Fig. 8. FTIR spectra of (a) Ru/TiO_2, (b) Ru—Ni/TiO_2, and (c) Ni/TiO_2 after CO_2 methanation for 60 min at 200 °C. These spectra were recorded after a switch from the model gas mixture for CO_2 methanation to 5% H_2/Ar.

with that of the monometallic Ni catalyst. They concluded from these results that on the bimetallic Ru—Ni catalyst most of the Ru species were covered by Ni species, which gave rise to the enhancement of the Ni reducibility. Li et al. reported the characterization of Nb_2O_5-supported Ni—Cu bimetallic catalysts [42]. Addition of Cu to Ni/Nb_2O_5 resulted in the decrease of reduction temperature of Ni species, measured by H_2-TPR. Only one reduction peak was detected in the H_2-TPR profile of $Ni—Cu/Nb_2O_5$, indicating the incorporation of Cu to Ni/Nb_2O_5 which is based on the facile formation of Ni—Cu alloy. In our case TEM in Fig. 3 observed Ru species on Ru—Ni/TiO_2 as particles, and the H_2-TPR in Fig. 4 indicated the Ru species existed as bimetallic clusters without forming alloys with the Ni species. Thus it is clear that the structure and morphology of Ru—Ni particles on our Ru—Ni bimetallic catalyst were different from those on the catalysts reported by Crisafulli et al. [40,41]. The third possibility is H_2 spillover from Ru to enhance NiO reduction. Dissociative hydrogen adsorption on a noble metal such as Ru, and the spillover to a near metal oxide to enable its reduction has been reported in several papers [23,43]. The reduction of NiO by spillover H_2 from metallic Ru requires close contact of Ni species with Ru metal. The TEM images (Fig. 3(d)–(f)) presented earlier provide evidence that Ru species on Ru—Ni/TiO_2 exist in contiguity with Ni species.

To obtain further insight on the reaction process the surface species during catalytic reactions on Ru/TiO_2, Ru—Ni/TiO_2, and Ni/TiO_2 were examined by Fourier transform infrared spectroscopy (FTIR) measurements. A model gas mixture for CO_2 methanation ($CO_2/H_2/N_2 = 2/15/83$) was used. It was observed that the interaction of CO_2 and H_2 with the catalyst surface at 200 °C gave rise to several bands located between 3100 and 1100 cm^{-1}. In the high wavenumber range peaks at 2960 and 2890 cm^{-1} appeared over Ru/TiO_2, Ru—Ni/TiO_2, and Ni/TiO_2, shown in Fig. 5. These can be assigned to C—H stretching modes in CH_3 groups and C—H vibration of surface formate, respectively [19–22]. There were no peaks assignable to CH_2 symmetric vibrations (at 2930 cm^{-1}) and asymmetric modes (at 2860 cm^{-1}) and this suggests that no chain growth of hydrocarbons occurred over these catalysts at these conditions [19–22].

Fig. 6 shows FTIR spectra of the Ru, Ru—Ni, and Ni monometallic and bimetallic catalysts after CO_2 methanation using model gas mixture, in the region between 2200 and 1100 cm^{-1}. On all catalysts two prominent bands appeared at around 1570 and 1365 cm^{-1}, assignable to formate peaks on the catalyst surface [17,19–22,44–47]. The formate peaks grew with increasing reaction time. Also on all catalysts adsorption peaks at 1620 and 1445 cm^{-1} were observed, which are attributed to carbonate species on the TiO_2 surface [17,19–22,44–47]. For Ru/TiO_2 and Ni/TiO_2 the carbonate peaks grew in intensity with increasing

reaction time, but for Ru—Ni/TiO_2 the carbonate peaks were almost constant during reaction for 60 min. On the Ru/TiO_2 catalyst a band can be seen at 1990 cm^{-1}, ascribed to linearly adsorbed CO on metallic Ru [17,19–22]. This result indicates that CO_2 was converted to CO over Ru/TiO_2 in the presence of H_2. The CO band was not present in the other catalysts. To summarize these results, strong formate and carbonate peaks were observed over Ru/TiO_2 and Ni/TiO_2, while over Ru—Ni/TiO_2 strong formate peaks and weak carbonate peaks were observed.

In order to assess the role of these species in the reaction transient experiments in N_2 and H_2/Ar atmosphere were undertaken. Under N_2 atmosphere the formate peaks were unchanged, as shown in Fig. 7. In addition, in H_2/Ar flow the formate peaks at 1580 and 1365 cm^{-1}, formed by the reaction of CO_2 and H_2, progressively decreased in intensity over the three catalysts, as illustrated in Fig. 8. These results show that formate species are thermally stable but react with H_2 at 200 °C over the TiO_2 supported Ru—Ni monometallic and bimetallic catalysts.

The formate species are regarded as intermediates adsorbed on the TiO_2 surface that are transformed into CO species in the vicinity of the metal particles [48,49]. The presence of large formate peaks on Ru—Ni/TiO_2 indicates that the decomposition of the formate species is slow over Ru—Ni/TiO_2, in contrast to Ru/TiO_2. This suppresses the conversion of CO_2 to CO.

4. Conclusions

In summary, the effect of combining Ru and Ni on TiO_2 on the activity and selectivity for CO methanation was investigated. The Ni component improved CO methanation and suppressed CO_2 methanation at low and high temperatures, respectively, leading to expansion of the temperature window for selective CO methanation with a shift to lower temperature. Consequently, the temperature window for selective CO methanation defined as CO concentration <500 ppm and CH_4 concentration <5000 ppm was expanded to 190–290 °C over Ru—Ni/TiO_2 from 200 to 285 °C over Ru/TiO_2. The reducibility of Ni species on Ru—Ni/TiO_2 was enhanced by the Ru species, which indicates that the Ni component existed in the proximity of Ru species. Transmission electron microscopy and X-ray energy dispersive spectrometry confirmed that Ru species were in close proximity to Ni on Ru—Ni/TiO_2. Additionally, the decomposition of formate species, known as a CO_2 methanation intermediate, on Ru—Ni/TiO_2 was suppressed compared to Ru/TiO_2, resulting in degradation of the conversion rate of CO_2 to CO. This was possibly because in Ru—Ni/TiO_2 most of the Ru species reside on Ni species and consequently the active interface between Ru and TiO_2 for CO_2 methanation was decreased.

Acknowledgments

This study was supported by New Energy and Industrial Technology Development Organization (NEDO). TEM observation was conducted in Center for Nano Lithography & Analysis, The University of Tokyo, supported by the Ministry of Education, Culture, Sports, Science and Technology, Japan.

References

[1] E. Antolini, Journal of Applied Electrochemistry 34 (2004) 563–576.
[2] E. Yoo, T. Okada, T. Kizuka, J. Nakamura, Electrochemistry 75 (2007) 146–148.
[3] T. Utaka, T. Okanishi, T. Takeguchi, R. Kikuchi, K. Eguchi, Applied Catalysis A: General 245 (2001) 343–351.
[4] P. Panagiotopoulou, D.I. Kondarides, Catalysis Today 112 (2006) 49–52.
[5] O. Goerke, P. Pfeifer, K. Schubert, Applied Catalysis A: General 263 (2004) 11–18.
[6] M. Echigo, T. Tabata, Catalysis Today 90 (2004) 269–275.
[7] F. Marino, C. Descorme, D. Duprez, Applied Catalysis B: Environmental 54 (2004) 59–66.
[8] S.H. Kim, S.-W. Nam, T.-H. Lim, H.-I. Lee, Applied Catalysis B: Environmental 81 (2008) 97–104.
[9] T. Tabakova, G. Avgouropoulos, J. Papavasiliou, M. Manzoli, F. Boccuzzi, K. Tenchev, F. Vindigni, T. Ioannides, Applied Catalysis B: Environmental 101 (2011) 256–265.
[10] M. Echigo, T. Tabata, Journal of Chemical Engineering of Japan 37 (2004) 75–81.
[11] P. Panagiotopoulou, D.I. Kondarides, X.E. Verykios, Applied Catalysis B: Environmental 88 (2009) 470–478.
[12] P. Panagiotopoulou, D.I. Kondarides, X.E. Verykios, Industrial & Engineering Chemistry Research 50 (2011) 523–530.
[13] C. Galletti, S. Specchia, G. Saracco, V. Specchia, Chemical Engineering Science 65 (2010) 590–596.
[14] S. Takenaka, T. Shimizu, K. Otsuka, International Journal of Hydrogen Energy 29 (2004) 1065–1073.
[15] P. Djinović, C. Galletti, S. Specchia, V. Specchia, Catalysis Today 164 (2011) 282–287.
[16] K. Urasaki, K. Endo, T. Takahiro, R. Kikuchi, T. Kojima, S. Satokawa, Topics in Catalysis 53 (2010) 707–711.
[17] P. Panagiotopoulou, D.I. Kondarides, X.E. Verykios, Journal of Physical Chemistry C 115 (2011) 1220–1230.
[18] K. Urasaki, Y. Tanpo, T. Takahiro, J. Christopher, R. Kikuchi, T. Kojima, S. Satokawa, Chemistry Letters 39 (2010) 972–973.
[19] S. Eckle, Y. Denkwitz, R.J. Behm, Journal of Catalysis 269 (2010) 255–268.
[20] S. Eckle, H.-G. Anfang, R.J. Behm, Applied Catalysis A: General 391 (2011) 325–333.
[21] S. Eckle, H.-G. Anfang, R.J. Behm, Journal of Physical Chemistry C 115 (2011) 1361–1367.
[22] S. Eckle, H.-G. Anfang, R.J. Behm, Catalysis Today 181 (2012) 40–51.
[23] A. Chen, T. Miyao, K. Higashiyama, H. Yamashita, M. Watanabe, Angewandte Chemie International Edition 49 (2010) 9895–9898.
[24] S. Tada, R. Kikuchi, K. Urasaki, S. Satokawa, Applied Catalysis A: General 404 (2011) 149–154.
[25] V. Jiménez, P. Sánchez, P. Panagiotopoulou, J.L. Valverde, A. Romero, Applied Catalysis A: General (2010) 35–44.
[26] F. Solymosi, I. Tombácz, M. Kocsis, Journal of Catalysis 75 (1982) 78–93.
[27] M. Araki, V. Ponec, Journal of Catalysis 44 (1976) 439–448.
[28] J. Kopyscinski, T.J. Schildhauer, F. Vogel, S.M.A. Biollaz, A. Wokaun, Journal of Catalysis 271 (2010) 262–279.
[29] I.A. Fisher, A.T. Bell, Journal of Catalysis 162 (1996) 54–65.
[30] W.H. Bragg, W.L. Bragg, in: W.L. Bragg (Ed.), The Crystalline State, G. Bell and Sons Ltd, London, 1962, pp. 188-207.
[31] T. Inui, M. Funabiki, Y. Takegami, Reaction Kinetics and Catalysis Letters 12 (1979) 287–290.
[32] D. Li, N. Ichikuni, S. Shimazu, T. Uematsu, Applied Catalysis A: General 180 (1999) 227–235.
[33] T. Mitsui, K. Tsutsui, T. Matsui, R. Kikuchi, K. Eguchi, Applied Catalysis B: Environmental 81 (2008) 56–63.
[34] L. Li, L. Qu, J. Cheng, J. Li, Z. Hao, Applied Catalysis B: Environmental 88 (2009) 224–231.
[35] V. Mazzieri, F. Coloma-Pascual, M. González, P.C. L'Argentière, N.S. Fígoli, Reaction Kinetics and Catalysis Letters 76 (2002) 53–59.
[36] P.M. Sreekanth, P.G. Smirniotis, Catalysis Letters 122 (2008) 37–42.
[37] Q.G. Yan, W.Z. Weng, H.L. Wan, H. Toghiani, R.K. Toghiani, C.U. PittmanJr., Applied Catalysis A: General 239 (2003) 43–58.
[38] J.P. Espinós, A.R. Gonzalez-Elipe, A. Caballero, J. García, G. Munuera, Journal of Catalysis 136 (1992) 415–422.
[39] D. Li, I. Atake, T. Shishido, Y. Oumi, T. Sano, K. Takehira, Journal of Catalysis 250 (2007) 299–312.
[40] C. Crisafulli, S. Scirè, R. Maggiore, S. Minicò, S. Galvagno, Catalysis Letters 59 (1999) 21–26.
[41] C. Crisafulli, S. Scirè, S. Minicò, L. Solarino, Applied Catalysis A: General 225 (2002) 1–9.
[42] J. Li, G. Lu, K. Li, W. Wang, Journal of Molecular Catalysis A: Chemical 221 (2004) 105–112.
[43] J.-N. Park, E.W. McFarland, Journal of Catalysis 266 (2009) 92–97.
[44] K.K. Bando, K. Sayama, H. Kusama, K. Okabe, H. Arakawa, Applied Catalysis A: General 165 (1997) 391–409.
[45] M. Haruta, S. Tsubota, T. Kobayashi, H. Kageyama, M.J. Genet, Journal of Catalysis 144 (1993) 175–192.
[46] C. Elmasides, D.I. Kondarides, W. Grünert, X.E. Verykios, Journal of Physical Chemistry B 103 (1999) 5227–5239.
[47] M. Kimura, T. Miyao, S. Komori, A. Chen, K. Higashiyama, H. Yamashita, M. Watanabe, Applied Catalysis A: General 379 (2010) 182–187.
[48] N.M. Gupta, V.S. Kamble, V.B. Kartha, R.M. Iyer, K.R. Thampi, M. Gratzel, Journal of Catalysis 146 (1994) 173–184.
[49] M. Marwood, R. Doepper, A. Renken, Applied Catalysis A: General 151 (1997) 223–246.